

TITLE: A Developmental Reduction of the Excitation:Inhibition Ratio in Association Cortex during Adolescence.

AUTHORS: Bart Larsen^{1,2*}, Zaixu Cui^{1,2}, Azeez Adebimpe^{1,2}, Adam Pines^{1,2}, Aaron Alexander-Bloch^{1,2}, Max Bertolero^{1,2}, Monica E. Calkins^{1,2}, Raquel E. Gur^{1,2,3}, Ruben C. Gur^{1,2,3}, Arun S. Mahadevan⁴, Tyler M. Moore^{1,2}, David R. Roalf^{1,2}, Jakob Seidlitz^{1,2}, Valerie J. Sydnor^{1,2}, Daniel H. Wolf^{1,2†}, Theodore D. Satterthwaite^{1,2†}

AFFILIATIONS:

¹Department of Psychiatry, University of Pennsylvania, Philadelphia, PA 19104, USA

²Penn/CHOP Lifespan Brain Institute, University of Pennsylvania, Philadelphia, PA 19104, USA

³Department of Radiology, University of Pennsylvania, Philadelphia, PA 19104, USA

⁴Department of Bioengineering, University of Pennsylvania, Philadelphia, PA 19104, USA

[†]Authors contributed equally

*Corresponding author: bart.larsen@pennmedicine.upenn.edu

KEYWORDS: adolescence; development; critical period; excitation; inhibition; GABA; functional connectivity; mood disorder

ABSTRACT

Adolescence is hypothesized to be a critical period for the development of association cortex. A reduction of the excitation:inhibition (E:I) ratio is a hallmark of critical period development; however it has been unclear how to measure the development of the E:I ratio using non-invasive neuroimaging techniques. Here, we used pharmacological fMRI with a GABAergic benzodiazepine challenge to empirically generate a model of E:I ratio based on multivariate patterns of functional connectivity. In an independent sample of 879 youth (ages 8-22 years), this model predicted reductions in the E:I ratio during adolescence, which were specific to association cortex and related to psychopathology. These findings support hypothesized shifts in E:I balance of association cortices during a neurodevelopmental critical period in adolescence.

MAIN

Adolescent brain development is characterized, in part, by the continued structural and functional maturation of the association cortices^{1–10}. The specificity of the developmental timing and localization of association cortex maturation as well as the links between association cortex development and long-term psychiatric outcomes have led to the hypothesis that adolescence functions as a critical period of development within association cortex^{11,12}. Critical periods are windows of development during which experience powerfully shapes the development of neural circuits through heightened experience-dependent plasticity with long-term impacts on behavior¹³. These important neurodevelopmental windows are theorized progress hierarchically throughout development, beginning in primary sensory cortices and sequentially advance to secondary and higher-order cortical areas^{13,14}. The neurobiological mechanisms that underlie critical periods are thought to be conserved across the cortex and have been carefully delineated in decades of work on early critical periods in sensory cortex^{13–16}.

One of the hallmark features of critical period development is the maturation of GABAergic inhibitory circuitry, particularly parvalbumin positive interneurons, leading to a reduction in the excitation to inhibition (E:I) ratio^{15,17}. The reduction of the E:I ratio leads to an increase in the signal-to-noise ratio of local circuit activity as inhibition suppresses the effect of spontaneous activity on circuit responses in favor of stimulus-evoked activity¹⁸. This essential mechanism has been shown to regulate the timing of critical period development across visual¹⁶, auditory¹⁹, and sensorimotor cortices²⁰. As such, if the adolescent critical period hypothesis is correct, a developmental reduction in the E:I ratio should unfold across adolescence within association cortex.

Evidence for E:I development in association cortex during adolescence has been largely limited to animal models. This work has suggested prefrontal GABAergic inhibitory circuitry undergoes significant modifications. Specifically, parvalbumin (PV) interneurons, a critical

component E:I maturation in sensory system critical periods, have been shown increase in prefrontal cortex during adolescence in the rat²¹ and non-human primate^{22–24}. At the same time, the expression of GABA_A receptor $\alpha 1$ subunits, which are primarily expressed on PV cells and support fast synaptic inhibition²⁵ as well as synaptic plasticity²⁶, also increase during adolescence in the prefrontal cortex of the non-human primate^{27,28}. These neurobiological changes lead to important functional increases in inhibitory signaling, effectively reducing the E:I ratio^{29,30}. Together, these findings are suggestive of critical period development and may indicate similar processes are unfolding in the human³¹. Translating these findings to human studies of development is crucial as disruptions to the E:I balance are hypothesized to play a significant role in the onset of psychiatric disorders^{32–34}. However, the extent to which these critical period mechanisms are present in association cortex during adolescence in the human remains largely unexplored. Corroborating evidence has been found in postmortem studies which demonstrate increases in PV³⁵ and GABA_A $\alpha 1$ expression³⁶, but it has been unclear how to measure developmental changes in the E:I ratio *in vivo* in humans using available neuroimaging techniques. This lack of *in vivo* measures has limited our ability to test the adolescent critical period hypothesis.

Here, we leveraged a pharmacological fMRI (phMRI) experiment using a GABAergic benzodiazepine challenge to empirically generate a model for the effect of inhibitory modulation of the E:I ratio on patterns of fMRI connectivity. We confirmed the biological validity of our empirical model by comparing the model features to known aspects of benzodiazepine pharmacology as well as a functional gradient that has been shown to reflect patterns of excitatory and inhibitory interneuron expression^{37,38}. We then applied our model to a large, independent developmental dataset to investigate E:I changes occurring in association cortex during adolescence. We hypothesized that patterns of functional connectivity would develop to reflect a reduction in the E:I ratio that is specific to association cortex.

RESULTS

An empirical model of the E:I ratio

Forty-three adult participants completed a double-blind, placebo-controlled phMRI study with the benzodiazepine alprazolam (86 sessions total). Alprazolam is a positive allosteric modulator that enhances the effect of GABA at GABA_A receptors, increasing inhibition and reducing the E:I ratio³⁹. Functional connectivity matrices were derived for placebo and drug phMRI sessions using a top performing pipeline that minimized the impact of motion artifact⁴⁰. A linear support vector machine (SVM) classifier was trained to distinguish placebo and drug sessions based on the multivariate patterns of functional connectivity (**Figure 1**, green pathway). Cross-validation and permutation testing revealed that the trained SVM identified drug vs. placebo sessions in left-out data far better than chance (AUC = .716, $p_{\text{permutation}} = .002$; **Figure 2a**). Sensitivity analyses confirmed that in-scanner head motion was not associated with our pharmacological manipulation or model performance (**Supplemental Figure 1**). The spatial pattern of estimated feature weights from the SVM model highlighted the contributions of subcortical regions, including the thalamus and amygdala, and also contributions throughout the cortex (**Figure 2b**).

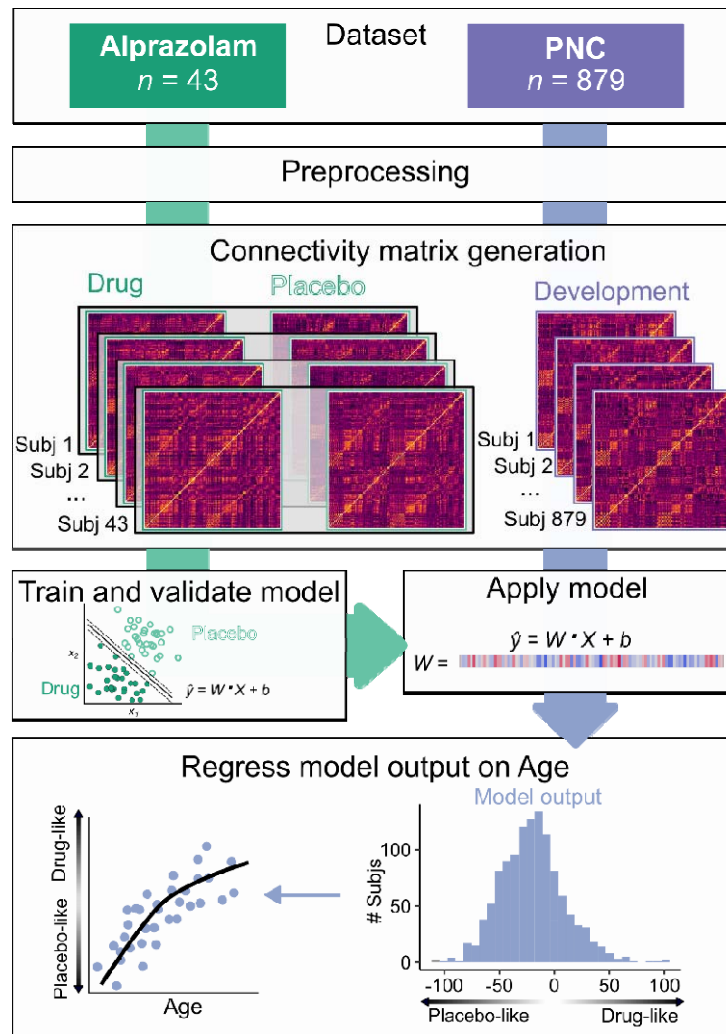


Figure 1. Analysis workflow. *Dataset:* Two datasets were collected on the same scanner using highly similar acquisition parameters: a phMRI dataset using the benzodiazepine alprazolam (green) and a developmental fMRI sample from the Philadelphia Neurodevelopmental Cohort (PNC; purple). *Preprocessing:* Datasets were preprocessed using identical pipelines which included removal of nuisance signal with aCompCor⁴¹, global signal regression, and task regression. *Connectivity matrix generation:* Connectivity matrices were generated from standard atlases for placebo and drug sessions from the alprazolam dataset ($n = 43$; 86 sessions total) and for the PNC dataset ($n = 879$). *Train and validate model:* The alprazolam dataset was used to train a linear SVM classifier to distinguish drug and placebo sessions using 10-fold cross-validation. *Apply model:* The validated alprazolam model was applied to the PNC dataset, generating a distance metric that reflected each participant's position on a continuum from "drug-like" (lower E:I) to "placebo-like" (higher E:I). *Regress model output on age:* This metric was then regressed on age using a generalized additive model with penalized splines that included covariates for sex, head motion, and attentiveness.

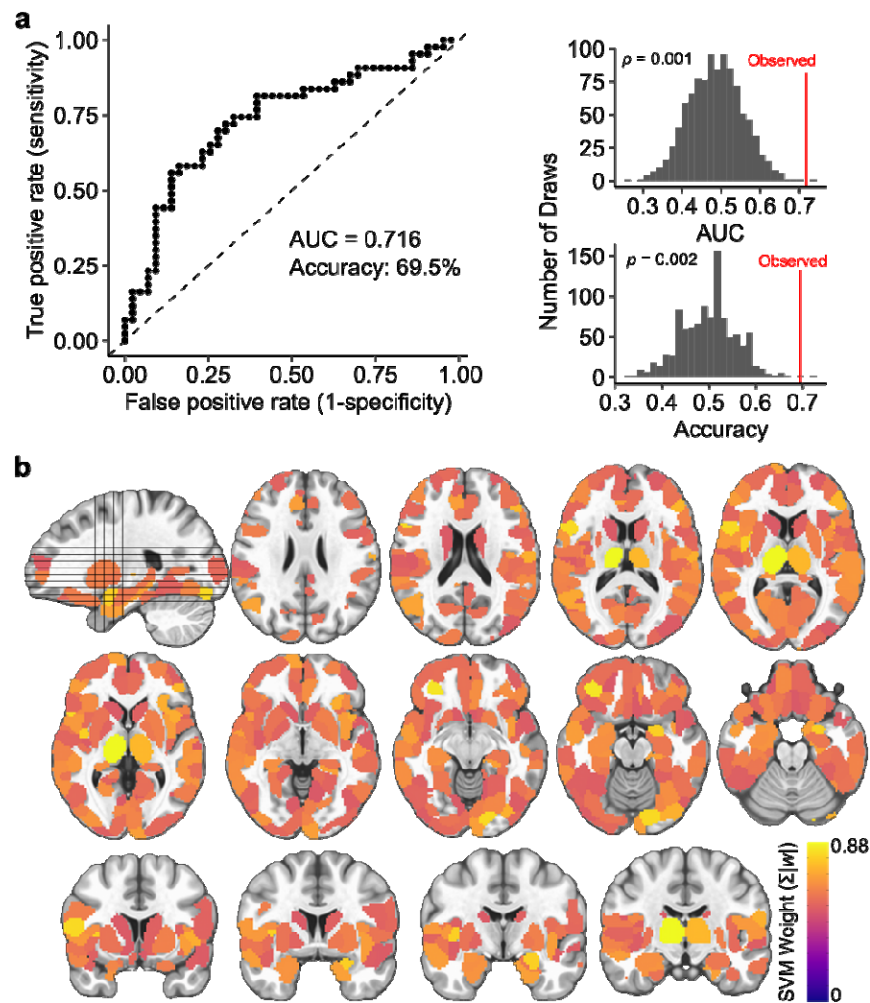


Figure 2. A multivariate model distinguishes alprazolam and placebo sessions, capturing E:I ratio **a)** Classifier performance. The binary SVM classifier identified drug and placebo sessions in 10-fold cross-validation with an AUC of .716 and an accuracy = 69.5% (top). The observed AUC and accuracy were significantly greater than a permuted null distribution (bottom). **b)** Mean absolute feature weights for all nodes from the validated SVM model. **c)** The cortical pattern of nodal SVM weights was significantly associated with transmodality using an established measure of macroscale cortical organization⁴². **d)** Nodal weights were also specifically correlated with the spatial patterns of benzodiazepine (BZD) sensitive GABA_A receptor subunit expression. Spatial relationships were tested for significance against a spatial-autocorrelation-preserving null distribution (BrainSMASH)⁴³.

Biological validity of the E:I model

Next, we established the biological validity of the trained E:I model. First, we compared the spatial pattern of cortical feature weights to a widely used functional gradient of macroscale cortical organization that places regions on a continuum from unimodal to transmodal function⁴². This continuum has been shown to capture variation in excitatory neuron structure, inhibitory interneuron expression, and excitatory to inhibitory neurotransmitter receptor density^{37,38}. Using a recently-developed analytic procedure that accounts for spatial autocorrelation structure⁴³, we observed a significant relationship between our model feature weights and this pattern of macroscale cortical organization ($r = .33$; $p = .003$; **Figure 3a**). This finding suggests that GABAergic modulation of functional connectivity patterns varies along a transmodal-to-unimodal gradient that in part indexes diversity in excitatory and inhibitory neurobiological properties. Next, we investigated whether the estimated model features corresponded to the known pharmacology of benzodiazepines like alprazolam. We used the Allen Human Brain Atlas⁴⁴ to evaluate whether feature weights in the classifier aligned with spatial patterns of gene expression for the six GABA_A subunit receptors, GABRA1-6 (corresponding to GABA_A α 1–6). Remarkably, we found evidence of a clear biological double dissociation: model features were significantly associated with the expression patterns of the benzodiazepine-sensitive GABA_A subunits (α 1,2,3,5) and not the benzodiazepine-*insensitive* GABA_A subunits (α 4, 6; **Figure 3b**)^{45,46}.

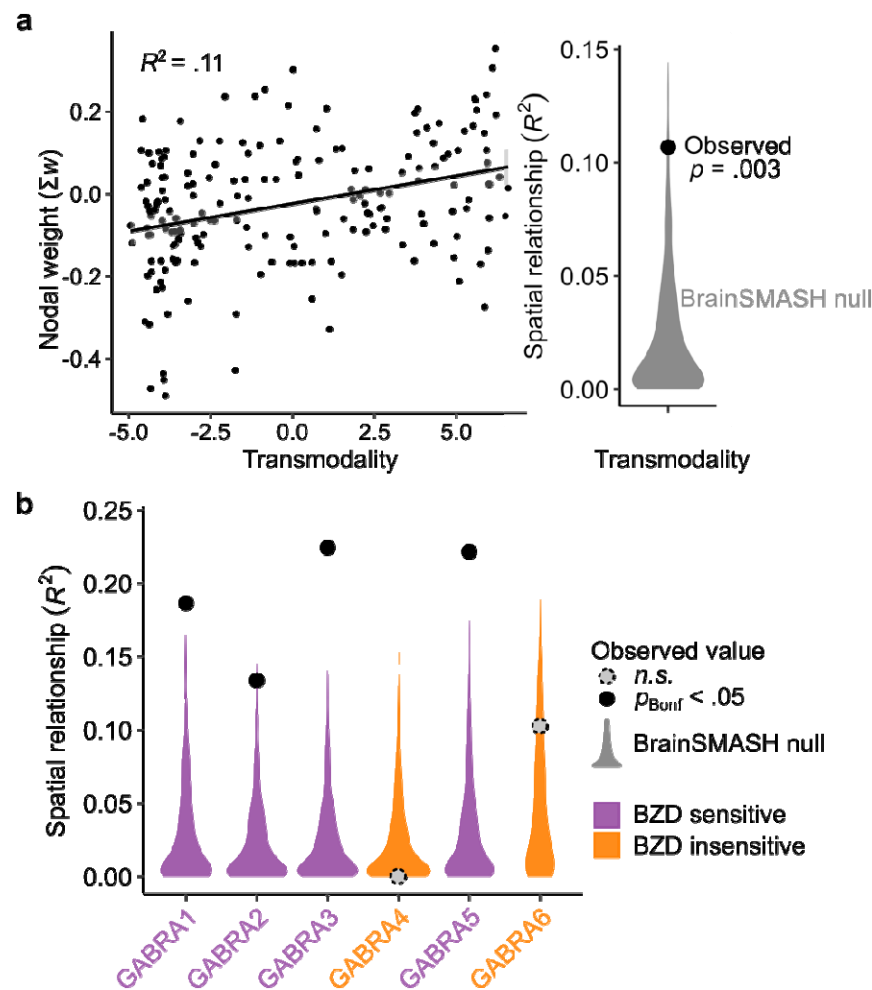


Figure 3. Model features align with cortical organization and benzodiazepine pharmacology **a)** The cortical pattern of nodal SVM weights from the multivariate E:I ratio model was significantly associated with transmodality using an established measure of macroscale cortical organization⁴². **b)** Nodal weights were also specifically correlated with the spatial patterns of benzodiazepine (BZD) sensitive GABA_A receptor subunit expression. Spatial relationships were tested for significance against a spatial-autocorrelation-preserving null distribution (BrainSMASH⁴³) and corrected for multiple comparison using the Bonferroni correction (p_{Bonf}).

Development of the E:I ratio during adolescence

We next utilized our empirically generated E:I ratio model to test the hypothesis that E:I ratio declines as part of the critical period of association cortex development. An independent sample of 879 youth (aged 8-21.7 years) participated in a highly similar fMRI acquisition on the same scanner; this data was preprocessed using an identical pipeline. We applied our validated E:I model to the developmental dataset without further tuning and obtained the model-estimated distance from the classification hyperplane. This metric reflects a participant's position on the continuum between “drug-like” (lower E:I) and “placebo-like” (higher E:I). To capture both linear and nonlinear effects in a rigorous statistical framework, we then regressed this metric on age using a generalized additive model with penalized splines (**Figure 1**, purple pathway). We found that age was positively associated with patterns of GABA-modulated functional connectivity, reflecting an age-related reduction in E:I ratio. Significant reductions occurred between ages 12.9 and 16.7 years ($F_{s(Age)} = 3.11$, $p = .037$; **Supplemental Table 1**, “All connections”). The age-related reduction in E:I ratio was robust across multiple alternative parcellation schemes (**Supplemental Table 2**; **Supplemental Figure 2**).

Age-related reductions in the E:I ratio are specific to association cortex

We hypothesized that age-related reductions in E:I ratio during adolescence were specific to association cortices. To test this hypothesis, we trained two additional models that restricted input features to connections to the most transmodal (**Figure 4a**, blue) or unimodal (**Figure 4a**, green) parts of the cortex. Both models significantly distinguished drug from placebo phMRI sessions (**Figure 4a**). However, when applied to the developmental dataset, significant age-related reductions in the E:I ratio were only observed for the model trained on connections with transmodal cortex (transmodal: $F_{s(Age)} = 9.96$, $p = .0017$; unimodal: $F_{s(Age)} = 3.59$, $p = .058$; transmodal vs. unimodal: $F_{s(Age)} = 5.96$, $p = .015$; **Figure 4b**). These results suggest that transmodal association cortices undergo a reduction in E:I ratio during adolescence, consistent

with a critical period of development.

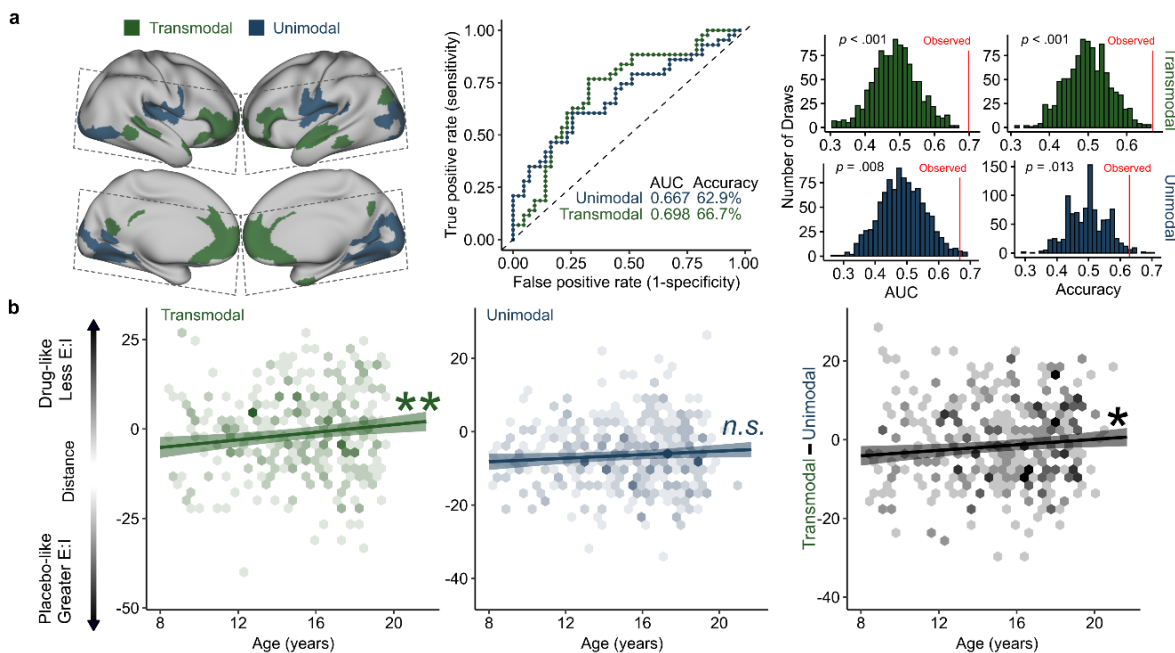


Figure 4. Transmodal areas undergo E:I ratio development during adolescence. a) Model performance for unimodal and transmodal classifiers. SVM classifiers were trained and validated for connections to the most transmodal (green) and most unimodal (blue) areas only. Dashed lines indicate acquisition field of view for the pHMRI dataset. Both models performed significantly better than a permuted null distribution (middle: ROC curves for each model; right: null distributions from 1,000 null permutations). **b)** Models trained on transmodal and unimodal data were applied to the developmental dataset, generating a distance metric for each participant where greater values represent patterns of functional connectivity consistent with a lower E:I ratio. Individuals had lower estimated E:I ratio with age in transmodal cortex (left) but not in unimodal cortex (center). This pattern was confirmed by a significant effect of age on within subject change in transmodal vs. unimodal distance scores (right). * $p < .05$, ** $p < .01$, n.s. not significant.

Analysis of dimensions of psychopathology

Finally, we investigated whether individual differences in dimensions of psychopathology⁴⁷ were associated with the E:I ratio of association cortex. We found that mood disorder symptomatology, but not other psychopathology dimensions, moderated age-related differences in estimated transmodal E:I ratio. Specifically, individuals with greater lifetime mood disorder symptoms displayed a relatively stable E:I ratio over development instead of the normative reduction of the E:I ratio (Age*Mood interaction: $F = 7.64$, $p = .0058$).

DISCUSSION

We utilized a unique combination of human pHMRI and developmental fMRI data to provide novel evidence for an essential component of critical period development: developmental reductions in the E:I ratio. Our approach generated an empirical fMRI model of the E:I ratio that showed a remarkable degree of correspondence to known GABAergic benzodiazepine neuropharmacology and which could be applied to a large, independent sample of youth. Consistent with our hypothesis, this approach revealed that patterns of functional neurodevelopment in adolescence are consistent with developmental reductions in the E:I ratio that are specific to association cortex. Further, we show that individual differences in this process are associated with individual differences in lifetime mood symptom burden, in alignment with models positing that E:I abnormalities underlie the emergence of psychopathology^{11,32,33,48–51}. Together, these findings support the hypothesis that critical period mechanisms shape association cortices during adolescence.

Critical period development has been predominantly associated with early sensory cortex development. Since the first studies of critical period development in the visual cortex almost 60 years ago^{52–54}, a wealth of prior work has elucidated the mechanisms that shape critical period plasticity in these areas. These studies have identified the maturation of local

inhibitory circuitry, particularly PV interneurons, and its resulting impact on the E:I balance as an essential critical period mechanism^{15,18}. This phenomenon is necessary for the opening of the critical period window, facilitates critical period plasticity, and is present in critical periods across sensory modalities^{18,19,26,55}. The results of this study suggest that this phenomenon also occurs in association cortex during human adolescence.

Our findings align with a growing literature characterizing inhibitory maturation during this developmental stage. Animal models and post mortem human studies have shown maturation of inhibitory neurobiology in the prefrontal cortex during adolescence, including increasing expression of PV interneurons and GABA_A $\alpha 1$ receptor subunits^{21,23,27,28}. These processes increase functional inhibition, reducing the E:I ratio and increasing the signal-to-noise ratio of circuit activity^{18,29,30,56}. Computational simulations have suggested that these maturational also facilitate high-frequency oscillatory capability³⁰. This is consistent with human EEG studies showing increased gamma-band oscillatory power during adolescence^{57,58}. Finally, two recent magnetic resonance spectroscopy studies have showed increases in GABA levels relative to glutamate levels in frontal cortex during adolescence^{59,60}. Though it is not possible to examine the functional effect of these changes on the E:I ratio using spectroscopy, these findings align with a model of developmental reduction in the E:I ratio during adolescence. This body of prior work cohere with the findings presented here, and are consistent with a critical period model of adolescent association cortex development. Just as sensory critical period plasticity refines neural circuits underlying sensory processing, the critical period for association cortex may facilitate the plasticity of circuits that underlie the higher-order cognitive processes refined during adolescence and are thought to be dependent on association cortex^{2,6,11}.

It should be noted that there are two classes of critical period mechanisms: *Facilitating factors* which open the critical period window and facilitate plasticity, and *braking factors* which stabilize neural circuits and physically limit future plasticity^{13,15}. The maturation of inhibition and

the resulting reduction in the E:I ratio are critical period facilitators¹³. Using generalized additive models, which can flexibly capture linear and nonlinear effects while penalizing overfitting, we found that the model fit for age-related reductions in the association cortex E:I ratio was linear. It is important to note that this does not necessarily mean that critical period plasticity is linearly increasing or that the critical period window is persistently open over the entire age range reported here. The developmental reduction in the E:I ratio is indicative of critical period opening, but it does not provide information about critical period closure. Closure of the adolescent critical period would be dependent upon the development of braking factors, such as myelination and the formation of perineuronal nets (PNN)^{61–63}, which may follow distinct developmental trajectories. Consistent with a critical period model, many studies have provided evidence of myelination of association cortex and large white matter pathways linking association cortex to other areas of the brain that continues into adulthood, including histological⁶⁴, myelin mapping^{65–69}, and diffusion imaging^{70–72}. At present, studies of PNN formation are limited to postmortem methods and animal models which have demonstrated developmental increases in PNN formation in the prefrontal cortex from adolescence to adulthood^{73–76}. Together, these studies indicate that critical period braking factors are forming during the transition from adolescence to adulthood, stabilizing neural circuits and closing the critical period window. However, in order to precisely demarcate the opening and closing of critical period plasticity during adolescence, future work is needed that jointly investigates the developmental timecourse of critical period facilitators, such as the E:I ratio reported here, and critical period braking factors.

Mood-related psychopathology typically first emerges during adolescence, with adolescent onset predicting greater illness chronicity and comorbidity^{77,78}. Here, we observed that beginning in adolescence, youth with greater burden of mood symptoms exhibit an altered trajectory of E:I development within the association cortex. Specifically, greater lifetime mood

symptom burden was associated with reduced development of inhibition in transmodal regions of the brain. Many studies have linked the occurrence of psychopathology with E:I disruption^{32,33,48,49,79}, and cross-species research has specifically implicated GABA-mediated E:I disruptions in the etiology of mood psychopathology^{80–82}. Specifically, animal studies have shown that initial reductions in GABAergic inhibition lead to downstream reductions in glutamatergic transmission, and to alteration of the normal E:I balance^{33,48,83}. Human studies have provided convergent evidence, demonstrating reduced GABA levels in the brain in those with depression⁸⁴ as well as reduced glutamate in individuals with more severe anhedonia⁸⁵. Conversely, the pharmacologic enhancement of GABAergic signaling within association regions has been shown to have antidepressant effects^{33,80,86}. As such, our study supports the hypothesis that the pathophysiology of depression in part involves altered glutamatergic and GABAergic signaling^{33,48}. Moreover, it places this hypothesis within a neurodevelopmental framework—underscoring how E:I disruptions can manifest due to atypical critical period development.

Finally, we note that the approach used in this study highlights the potential for phMRI data to generate insights into independent datasets to inform new hypotheses. We combined machine learning and phMRI using a GABAergic alprazolam challenge to generate an empirical model for the effect of GABAergic modulation on patterns of fMRI connectivity. As evidence for the efficacy of this approach, the trained model could not only significantly predict drug versus placebo sessions in unseen data, but the model features demonstrated a remarkable correspondence with known benzodiazepine neuropharmacology. Notably, the model features were significantly associated with the GABA receptor most strongly implicated in critical period development, the GABA_A $\alpha 1$ receptor. The model performance and underlying interpretability of the learned features highlights the biological validity of this method. Whereas in this study we applied this method to an independent developmental dataset to provide insights into the critical

period mechanisms unfolding during adolescence, future work could apply this approach to other datasets to inform new research questions.

Together, these findings support the hypothesis that critical period mechanisms, such as the reduction of the E:I ratio, shape association cortices during adolescence. Studying development from a critical period perspective provides a powerful mechanistic framework for understanding how experience and neurobiology interact to shape long-term cognitive, social, and psychiatric outcomes. Importantly, a critical period model of adolescent development can draw on the history of detailed work on sensory critical periods to generate testable hypotheses for the mechanisms unfolding during adolescence in association cortex. Understanding these mechanisms are a necessary prerequisite to understanding of how experience, environment, and neurobiology contribute to differing neurodevelopmental trajectories in health and mental illness. This work thus lays the groundwork for future studies of the unique impact of experience on neurodevelopment and also suggests the possibility of targeted interventions during this critical window of vulnerability to psychopathology^{34,87}.

METHODS

Participants and experimental procedures

Alprazolam sample

The alprazolam sample and study procedures have been described in detail in our earlier work⁸⁸. Briefly, forty-seven adults participated in a double-blind, placebo controlled pharmacological imaging study using the benzodiazepine alprazolam. Each participant completed two identical experimental sessions approximately one week apart. In one session, participants were given a 1 mg dose of alprazolam, and in the other they were given an identical appearing placebo. The order of administration was counter-balanced across participants. During both sessions, participants completed an emotion identification task that lasted 10.5 minutes while functional MRI (fMRI) data was collected. Task-related fMRI results have been previously reported⁸⁸. Four participants were excluded due to excess head motion in at least one session (see below) for a final sample of 43 participants and 86 sessions total (ages 20.9 - 59.4; $M = 40.3$, $SD = 13.12$, male/female = 24/19). Study procedures were approved by the University of Pennsylvania IRB, and all participants provided written informed consent.

Developmental sample

Neuroimaging data were obtained from a community-based sample of 1,476 youth (ages 8 – 21.9, $M = 14.63$, $SD = 3.43$; male/female = 698/778) that were part of the Philadelphia Neurodevelopmental Cohort (PNC). Data collection procedures and sample characteristics have been previously described in detail^{47,89,90}. Functional MRI data were collected while participants performed the same emotion identification task as the alprazolam sample; this is also described in previous work⁸⁹. From this original sample, 306 participants were excluded based on health criteria, including psychoactive medication use at the time of study, medical problems that could impact brain function, a history of psychiatric hospitalization, and gross structural brain

abnormalities. A total of 234 participants were excluded from further analysis due to head motion (see below) and 56 were excluded for poor structural image quality. In sum, following health exclusions and rigorous quality assurance, we retained 879 participants (ages 8.0 - 21.7 at first visit, $M = 14.95$, $SD = 3.24$; male/female = 383/496).

Neuroimaging acquisition

Alprazolam sample

All data were collected on a Siemens Trio 3T as previously reported⁸⁸. Whole-brain structural data were obtained with a 5-minute magnetization-prepared, rapid acquisition gradient-echo T1-weighted image (MPRAGE) using the following parameters: TR 1620ms, TE 3.87 ms, field of view (FOV) 180x240 mm, matrix 192x256, effective voxel resolution of 1 x 1 x 1mm. BOLD fMRI data were obtained as a slab single-shot gradient-echo (GE) echoplanar imaging (EPI) sequence using the following parameters: TR = 3000, TE = 32 ms, flip angle = 90°, FOV = 240 mm, matrix = 128 X 128, slice thickness/gap = 2/0mm, 30 slices, effective voxel resolution of 1.875 x 1.875 x 2mm, 210 volumes. As previously described⁸⁸, data were acquired in a FOV that included temporal, inferior frontal, and visual cortices as well as subcortical structures (**Figure 3a**; gray boxes).

Developmental sample

All neuroimaging data were collected on the same Siemens Trio 3T scanner as was used for the alprazolam dataset. The neuroimaging procedures and acquisitions parameters have been previously described in detail⁸⁹. Briefly, structural MRI was acquired with a 5-min MPRAGE T1-weighted image (TR = 1810 ms; TE = 3.51 ms; TI = 1100 ms, FOV = 180 x 240 mm², matrix = 192 x 256, effective voxel resolution = 0.9 x 0.9 x 1 mm³). BOLD fMRI was acquired using similar acquisition parameters to the alprazolam dataset. BOLD fMRI scans were

acquired as single-shot, interleaved multi-slice, GE-EPI sequence sensitive to BOLD contrast with the following parameters: TR = 3000 ms, TE = 32 ms, flip angle = 90°, FOV = 192 × 192 mm² (whole brain acquisition), matrix = 64 × 64; 46 slices, slice thickness/gap = 3/0 mm, effective voxel resolution = 3.0 × 3.0 × 3.0 mm³, 210 volumes.

Preprocessing of neuroimaging data

All preprocessing was performed using fMRIPrep 20.0.7 (RRID:SCR_016216;⁹¹, which is based on Nipype 1.4.2⁹², and XCP Engine (PennBBL/xcpEngine: atlas in MNI2009 Version 1.2.3; Zenodo: <http://doi.org/10.5281/zenodo.4010846>; ^{40,93}. The neuroimaging data from the alprazolam and developmental datasets were processed using identical pipelines as described below.

Anatomical data preprocessing

The T1-weighted (T1w) image was corrected for intensity non-uniformity (INU) with N4BiasFieldCorrection⁹⁴, distributed with ANTs 2.2.0⁹⁵, and used as T1w-reference throughout the workflow. The T1w-reference was then skull-stripped with a Nipype implementation of the antsBrainExtraction.sh workflow (from ANTs), using OASIS30ANTs as target template. Brain tissue segmentation of cerebrospinal fluid (CSF), white-matter (WM) and gray-matter (GM) was performed on the brain-extracted T1w using FAST in FSL 5.0.9⁹⁶. Volume-based spatial normalization to MNI2009c standard space was performed through nonlinear registration with antsRegistration (ANTs 2.2.0), using brain-extracted versions of both the T1w reference and the T1w template.

Functional data preprocessing

The alprazolam dataset consisted of two BOLD acquisitions per participant (drug and placebo session) which were preprocessed individually. The developmental dataset consisted of one BOLD acquisition per participant. All BOLD acquisitions were processed with the following

steps. BOLD runs were first slice-time corrected using 3dTshift from AFNI 20160207⁹⁷ and then motion corrected using mcflirt (FSL 5.0.9;⁹⁶). A fieldmap was estimated based on a phase-difference map calculated with a dual-echo GRE sequence, processed with a custom workflow of SDCFlows inspired by the [epidewarp.fsl script](#) and further improvements in HCP Pipelines⁹⁸. The fieldmap was then co-registered to the target EPI reference run and converted to a displacement field map with FSL's fugue and other SDCflows tools. Based on the estimated susceptibility distortion, a corrected BOLD reference was calculated for a more accurate co-registration with the anatomical reference. The BOLD reference was then co-registered to the T1w reference using bbregister (FreeSurfer) which implements boundary-based registration⁹⁹. Co-registration was configured with nine degrees of freedom to account for distortions remaining in the BOLD reference. Six head-motion parameters (corresponding rotation and translation parameters) were estimated before any spatiotemporal filtering using mcflirt. Finally, the motion correcting transformations, field distortion correcting warp, BOLD-to-T1w transformation and T1w-to-template (MNI) warp were concatenated and applied to the BOLD timeseries in a single step using antsApplyTransforms (ANTs) with Lanczos interpolation.

Confounding time-series were calculated based on the preprocessed BOLD data. The global signal was extracted within the whole-brain mask. Additionally, a set of physiological regressors were extracted to allow for component-based noise correction (CompCor, Behzadi et al. 2007). Anatomical CompCor (aCompCor) principal components were estimated after high-pass filtering the preprocessed BOLD time-series (using a discrete cosine filter with 128s cut-off). The aCompCor components were calculated within the intersection of the aforementioned mask and the union of CSF and WM masks calculated in T1w space, after their projection to the native space of each functional run (using the inverse BOLD-to-T1w transformation). Components were also calculated separately within the WM and CSF masks. In this study, for each aCompCor decomposition, the k components with the largest singular values were

retained, such that the retained components' time series were sufficient to explain 50 percent of variance across the nuisance mask (CSF and WM). The remaining components were dropped from consideration. The head-motion estimates calculated in the correction step were also placed within the corresponding confounds file. The confound time series derived from head motion estimates and global signals were expanded with the inclusion of temporal derivatives and quadratic terms for each¹⁰⁰.

Subject-level timeseries analysis was carried out in XCP Engine using FILM (FMRIB's Improved General Linear Model)¹⁰¹. All event conditions from the emotion identification task^{88,89} were modeled in the GLM as 5.5 second boxcars convolved with a canonical hemodynamic response function. Each of the five emotions (fear, sad, angry, happy, neutral) was modeled as a separate regressor. The temporal derivatives and quadratic terms for each task condition as well as the confounding aCompCor, global signal, and motion timeseries described above were included as nuisance regressors. Task regression has been shown to produce patterns of BOLD fMRI connectivity that are highly similar to those present at rest¹⁰², and convergent results from several independent studies that have shown that functional networks are primarily defined by individual-specific rather than task-specific factors (Gratton et al., 2018). The nuisance regression pipeline used here has been shown to be a top-performing procedure for mitigating motion artifacts⁴⁰. Consistent with our prior work, participants in the alprazolam dataset were excluded from future analyses if mean framewise displacement exceeded 0.5 mm in either session. A more stringent threshold of 0.3 mm was applied to the developmental dataset; head motion was also included as a covariate in all developmental models (see below).

Connectivity matrix generation

Fully preprocessed fMRI data were used to generate mean timeseries within a set of atlas-defined brain regions for each participant. Cortical regions were defined according to the

Schaefer 400 parcel cortical atlas¹⁰³. To accommodate the restricted FOV of the alprazolam BOLD acquisition, the atlas was masked such that only parcels with greater than 95% coverage were included in connectivity analyses. Subcortical regions were defined using the Automated Anatomical Labeling (AAL) atlas¹⁰⁴. Subcortical areas included the left and right caudate, putamen, accumbens, pallidum, thalamus, amygdala, hippocampus, and parahippocampal area. These cortical and subcortical atlases were combined and used to generate mean timeseries for each region in each dataset. Functional connectivity was calculated as the correlation coefficient of the timeseries for each pair of regions (20,503 unique pairs). As part of sensitivity analyses, we repeated this process after defining cortical areas using Schaefer 200 parcellation¹⁰³, the Multi-modal Parcellation atlas¹⁰⁵, the Gordon cortical atlas¹⁰⁶, or the AAL¹⁰⁴.

Pharmacological classification analysis

We used a linear support vector machine (SVM) to classify drug vs. placebo sessions in the alprazolam dataset based on multivariate patterns of functional connectivity. Linear SVMs find a hyperplane to separate two classes of data by maximizing the margin between the closest points (the support vectors;¹⁰⁷. SVMs were implemented in R using the e1071 library¹⁰⁹ and were trained using a linear kernel and the default parameters. Model performance was evaluated using 10-fold cross-validation, iteratively selecting data from 90% of participants as training data and testing the trained model on data from the remaining 10% of participants. Across testing sets, the prediction accuracy and area under the receiver operating curve (AUC) were calculated to evaluate model performance. To ensure our results were not driven by a specific cross-validation split, we repeated the entire 10-fold cross-validation procedure 100 times, drawing the 10-fold subsets at random each time. Performance metrics were finally averaged across the 100 iterations of the cross-validation procedure.

To evaluate if model performance (i.e., the accuracy and the AUC) was significantly better than expected by chance, we performed a permutation test¹¹⁰. Specifically, we re-applied the cross-validation procedure 1,000 times, each time permuting the session labels (drug and placebo) across the training samples without replacement. Significance was determined by ranking the actual prediction accuracy versus the permuted distribution; the *p*-value of the accuracy and AUC was calculated as the proportion of permutations that showed a higher value than the observed value in the real, unpermuted data.

Analysis of feature weights

After cross-validation and significance testing, we trained the model on all participants and extracted the feature weights for further analysis. First, we calculated the absolute value of the weights and summed them across all connections (edges) for a given region (node) to compare the overall contribution of each region to the model, irrespective of the sign of the feature weights¹¹⁰. Next, to evaluate the spatial pattern of the feature weights, we calculated the mean signed feature weight for each node, reflecting the directionality of the effect of the drug manipulation according to the trained model. We then used this feature map to assess the biological validity of our trained model. Specifically, we calculated the spatial correlation between this pattern of nodal feature weights with two sets of cortical features. The first was the widely used principal gradient of macroscale cortical organization⁴², which places each cortical region on a continuum between unimodal (i.e. sensorimotor cortices) to transmodal (i.e. association cortices) function. The second set of cortical features was selected based on the known pharmacology of benzodiazepines like alprazolam. Alprazolam is a positive allosteric modulator of the GABA_A receptor, and of the six GABA_A α subunits (α 1-6), only subunits α 1, α 2, α 3, and α 5 are benzodiazepine sensitive^{46,111}. To quantify the spatial distribution of the six GABA_A α subunits, we extracted the microarray gene expression patterns for their corresponding GABA_A receptor genes (GABRA1-6) from the Allen Human Brain Atlas (data

available at <https://www.meduniwien.ac.at/neuroimaging/mRNA.html>)^{44,112}. For each of the six gene expression maps, we quantified the mean expression value within each cortical parcel and calculated the spatial correlation with the pattern of nodal SVM weights.

To test the significance of the spatial correlation between our pattern of cortical feature weights and each of the biological brain maps, we compared the observed correlation value to a null distribution generated with BrainSMASH (Brain Surrogate Maps with Autocorrelated Spatial Heterogeneity; <https://brainsmash.readthedocs.io/>;⁴³). The spatial autocorrelation of brain maps can lead to inflated *p*-values in spatial correlation analyses and must be accounted for in the creation of null models. BrainSMASH addresses this by generating permuted null brain maps that match the spatial autocorrelation properties of the input data. We used BrainSMASH to generate 10,000 spatial-autocorrelation-preserving null permutations based on the input data and the pairwise distance matrix for the cortical parcellation, generating a null distribution of spatial correlation coefficients. We calculated two-tailed *p*-values by squaring all correlation values (i.e. spatial R^2) and calculating the proportion of times the null distribution exceeded the observed value.

Transmodal and unimodal classification models

Our primary hypothesis was that E:I ratio reductions would be specific to association cortices during youth. In order to test this hypothesis directly, we trained two additional models after applying an *a priori* feature selection step. Specifically, we thresholded the top and bottom quartiles of cortical parcels based on their position in the principal gradient of functional organization⁴², with the top 25% representing transmodal association cortex and the bottom 25% representing unimodal sensory cortex. We then created two new feature sets that restricted the input features to connections to these transmodal or unimodal areas only. This selection procedure ensured that the resulting numbers of features were equal between the two

feature sets (9,541 features per model). We then trained and validated the transmodal and unimodal models according the procedures described above.

Developmental analyses

Application of the pharmacological model to the developmental dataset

After training and validating the pharmacological benzodiazepine models, we applied the models to the functional connectivity data for each participant in the developmental sample. For each participant, each model yielded the distance from the classification hyperplane that separates the two classes (drug vs. placebo). Observations close to the hyperplane (distance values near zero) are less representative of the class, and those further from the hyperplane are more representative. The distance metric is such that values greater than zero indicate more “drug-like” patterns of functional connectivity and values less than zero indicate more “placebo-like” patterns of connectivity. As the pharmacological effect of alprazolam is to increase GABAergic inhibitory signaling, more “drug-like” patterns reflect greater GABA-ergic inhibitory modulation of functional connectivity. As such, more “drug-like” patterns were interpreted to reflect a reduced E:I balance relative to more “placebo-like” patterns. These distance metrics were normally distributed and thus provided a continuous measure of E:I balance for use in further analyses. We first applied the model trained on all the input features and then applied the transmodal- and unimodal-specific models, generating three sets of distance values per participant.

Developmental regression models

To assess the developmental trajectory of E:I balance, we modeled the classification distance metrics from each model as a function of age using penalized splines within a generalized additive model (GAM). GAMs allow us to flexibly capture linear or nonlinear age effects while penalizing overfitting. To test for windows of significant change across the age

range, we calculated the first derivative of the smooth function of age from the GAM model using finite differences and then generated a simultaneous 95% confidence interval of the derivative following the method described by Simpson¹¹³ and implemented using the *gratia* library¹¹⁴ in R. Intervals of significant change were identified as areas where the simultaneous confidence interval of the derivative does not include zero. To test if the effect of age on classification distance differed between the transmodal and unimodal SVM models, we calculated the residualized change¹¹⁵ in transmodal vs. unimodal distance scores by regressing the unimodal distance out of transmodal distance. We then regressed the residualized change score on age using a GAM. All models included sex as a covariate as well as head motion and attentiveness as covariates of no interest. Head motion was quantified as mean framewise displacement during the fMRI acquisition. Attentiveness was quantified as the number of response omissions during the emotion identification task; this covariate was included to control for potential effects of arousal on model performance as alprazolam can cause drowsiness. All GAMs were fit using the *mgcv* library¹¹⁶ in R.

Analysis of dimensions of psychopathology

As previously described^{47,117,118}, PNC participants underwent a clinical assessment of psychopathology. Multiple domains of psychopathology symptoms were evaluated using a structured screening interview (GOASSESS); we used this data to investigate whether dimensions of psychopathology moderated developmental reductions in E:I balance. As has been detailed in prior work^{47,117,118}, factor scores were derived from the clinical assessments using a bifactor confirmatory factor analysis model that included a general factor for overall psychopathology as well as four specific factors that primarily represent anxious-misery (mood & anxiety) symptoms, psychosis-spectrum symptoms, behavioral symptoms (conduct and ADHD), and fear symptoms (phobias). Importantly, all five factors are orthogonal and can be considered jointly in analysis of imaging data. In order to sample a broad range of factor scores,

we expanded our inclusion criteria to include individuals with a history of psychiatric hospitalization ($N = 1018$; ages 8 – 21.7; $M = 15.0$, $SD = 3.23$, male/female = 462/556). We analyzed these data in a GAM that included age-by-factor score interactions for each factor from the bifactor model. Interactions were fit as bivariate smooth interactions with penalized splines using tensor interaction smooths (`ti`` in `mgcv`).

Data and code availability

The developmental dataset is publicly available in the Database of Genotypes and Phenotypes (dbGaP accession [phs000607.v3.p2](https://www.ncbi.nlm.nih.gov/gap/study/PHS000607.v3.p2)). Pharmacological imaging data is available upon reasonable request. All code used for pharmacological classification analyses and developmental analyses are available at https://pennlinc.github.io/Larsen_EI_Development/.

ACKNOWLEDGEMENTS

This study was supported by T32MH014654 to Dr. Larsen; R01MH112847, R01MH113550, RF1MH116920, and R01MH120482 to Dr. Satterthwaite; R01MH113565 to Dr. Wolf; R01MH117014 for Drs. R.C.G. and T.M.M.; R01 MH119185, R01 MH120174, R56 AG066656 for Dr. Roalf; F31MH123063 for Mr. Pines; K08MH120564 for Dr. Alexander-Bloch; and National Science Foundation Graduate Research Fellowship (DGE-1845298) for Ms. Sydnor.

Thanks to James Loughhead, Mark Elliott, Jeff Valdez, and Eve Overton for their assistance with data acquisition.

AUTHOR CONTRIBUTIONS

B.L. and T.D.S. conceived and designed the analyses. B.L., Z.C., and A.A. analyzed the data. J.S., A.P., M.B., and T.M.M contributed analysis tools. A.A.B., D.R.R., V.J.S., R.E.G., R.C.G., A.S.M., M.E.C., A.P., and M.B. commented on analyses. B.L. wrote the paper with contributions from all authors. T.D.S. and D.H.W. supervised the work.

DECLARATION OF INTERESTS

The authors declare no competing interests.

REFERENCES

1. Blakemore, S.-J. & Choudhury, S. Development of the adolescent brain: implications for executive function and social cognition. *Journal of Child Psychology and Psychiatry* **47**, 296–312 (2006).
2. Luna, B., Marek, S., Larsen, B., Tervo-Clemmens, B. & Chahal, R. An Integrative Model of the Maturation of Cognitive Control. *Annual Review of Neuroscience* **38**, 151–170 (2015).
3. Shanmugan, S. & Satterthwaite, T. D. Neural Markers of the Development of Executive Function: Relevance for Education. *Curr Opin Behav Sci* **10**, 7–13 (2016).
4. Cui, Z. *et al.* Individual Variation in Functional Topography of Association Networks in Youth. *Neuron* (2020) doi:10.1016/j.neuron.2020.01.029.
5. Satterthwaite, T. D. *et al.* Impact of puberty on the evolution of cerebral perfusion during adolescence. *PNAS* **111**, 8643–8648 (2014).
6. Satterthwaite, T. D. *et al.* Functional maturation of the executive system during adolescence. *J. Neurosci.* **33**, 16249–16261 (2013).
7. Velanova, K., Wheeler, M. E. & Luna, B. The Maturation of Task Set-Related Activation Supports Late Developmental Improvements in Inhibitory Control. *J. Neurosci.* **29**, 12558–12567 (2009).
8. Marek, S., Hwang, K., Foran, W., Hallquist, M. N. & Luna, B. The Contribution of Network Organization and Integration to the Development of Cognitive Control. *PLoS Biol* **13**, e1002328 (2015).
9. Gennatas, E. D. *et al.* Age-Related Effects and Sex Differences in Gray Matter Density, Volume, Mass, and Cortical Thickness from Childhood to Young Adulthood. *J. Neurosci.* **37**, 5065–5073 (2017).

10. Gogtay, N. & Thompson, P. M. Mapping gray matter development: Implications for typical development and vulnerability to psychopathology. *Brain Cogn In Press, Corrected Proof*, (2009).
11. Larsen, B. & Luna, B. Adolescence as a neurobiological critical period for the development of higher-order cognition. *Neuroscience & Biobehavioral Reviews* **94**, 179–195 (2018).
12. Crews, F., He, J. & Hodge, C. Adolescent cortical development: a critical period of vulnerability for addiction. *Pharmacol. Biochem. Behav.* **86**, 189–199 (2007).
13. Takesian, A. E. & Hensch, T. K. Balancing plasticity/stability across brain development. *Prog. Brain Res.* **207**, 3–34 (2013).
14. Reh, R. K. *et al.* Critical period regulation across multiple timescales. *PNAS* **117**, 23242–23251 (2020).
15. Hensch, T. K. Critical period plasticity in local cortical circuits. *Nature Reviews Neuroscience* **6**, 877–888 (2005).
16. Levelt, C. N. & Hübener, M. Critical-period plasticity in the visual cortex. *Annu. Rev. Neurosci.* **35**, 309–330 (2012).
17. Hensch, T. K. & Fagiolini, M. Excitatory–inhibitory balance and critical period plasticity in developing visual cortex. *Progress in Brain Research* **147**, 115–124 (2005).
18. Toyozumi, T. *et al.* A Theory of the Transition to Critical Period Plasticity: Inhibition Selectively Suppresses Spontaneous Activity. *Neuron* **80**, 51–63 (2013).
19. Takesian, A. E., Bogart, L. J., Lichtman, J. W. & Hensch, T. K. Inhibitory circuit gating of auditory critical-period plasticity. *Nature Neuroscience* **21**, 218–227 (2018).
20. Erzurumlu, R. S. & Gaspar, P. Development and critical period plasticity of the barrel cortex. *Eur. J. Neurosci.* **35**, 1540–1553 (2012).
21. Caballero, A., Flores-Barrera, E., Cass, D. K. & Tseng, K. Y. Differential regulation of parvalbumin and calretinin interneurons in the prefrontal cortex during adolescence. *Brain Struct Funct* **219**, 395–406 (2014).

22. Erickson, S. L. & Lewis, D. A. Postnatal development of parvalbumin- and GABA transporter-immunoreactive axon terminals in monkey prefrontal cortex. *J. Comp. Neurol.* **448**, 186–202 (2002).
23. Hoftman, G. D. *et al.* Altered cortical expression of GABA-related genes in schizophrenia: illness progression vs developmental disturbance. *Schizophr Bull* **41**, 180–191 (2015).
24. Hoftman, G. D. & Lewis, D. A. Postnatal Developmental Trajectories of Neural Circuits in the Primate Prefrontal Cortex: Identifying Sensitive Periods for Vulnerability to Schizophrenia. *Schizophr Bull* **37**, 493–503 (2011).
25. Bosman, L. W. J., Rosahl, T. W. & Brussaard, A. B. Neonatal development of the rat visual cortex: synaptic function of GABAA receptor alpha subunits. *J Physiol* **545**, 169–181 (2002).
26. Katagiri, H., Fagiolini, M. & Hensch, T. K. Optimization of somatic inhibition at critical period onset in mouse visual cortex. *Neuron* **53**, 805–812 (2007).
27. Hashimoto, T. *et al.* Protracted Developmental Trajectories of GABAA Receptor $\alpha 1$ and $\alpha 2$ Subunit Expression in Primate Prefrontal Cortex. *Biol Psychiatry* **65**, 1015–1023 (2009).
28. Datta, D., Arion, D. & Lewis, D. A. Developmental Expression Patterns of GABAA Receptor Subunits in Layer 3 and 5 Pyramidal Cells of Monkey Prefrontal Cortex. *Cereb Cortex* **25**, 2295–2305 (2015).
29. Piekarski, D. J., Boivin, J. R. & Wilbrecht, L. Ovarian Hormones Organize the Maturation of Inhibitory Neurotransmission in the Frontal Cortex at Puberty Onset in Female Mice. *Curr. Biol.* **27**, 1735-1745.e3 (2017).
30. Gonzalez-Burgos, G. *et al.* Functional Maturation of GABA Synapses During Postnatal Development of the Monkey Dorsolateral Prefrontal Cortex. *Cereb. Cortex* bhu122 (2014) doi:10.1093/cercor/bhu122.
31. Caballero, A. & Tseng, K. Y. GABAergic function as a limiting factor for prefrontal maturation during adolescence. *Trends Neurosci* **39**, 441–448 (2016).
32. Anticevic, A. & Murray, J. D. Rebalancing Altered Computations: Considering the Role of

Neural Excitation and Inhibition Balance Across the Psychiatric Spectrum. *Biological Psychiatry* **81**, 816–817 (2017).

33. Duman, R. S., Sanacora, G. & Krystal, J. H. Altered Connectivity in Depression: GABA and Glutamate Neurotransmitter Deficits and Reversal by Novel Treatments. *Neuron* **102**, 75–90 (2019).
34. Tang, X., Jaenisch, R. & Sur, M. The role of GABAergic signalling in neurodevelopmental disorders. *Nature Reviews Neuroscience* 1–18 (2021) doi:10.1038/s41583-021-00443-x.
35. Fung, S. J. *et al.* Expression of interneuron markers in the dorsolateral prefrontal cortex of the developing human and in schizophrenia. *American Journal of Psychiatry* **167**, 1479–88 (2010).
36. Duncan, C. E. *et al.* Prefrontal GABA(A) receptor alpha-subunit expression in normal postnatal human development and schizophrenia. *J Psychiatr Res* **44**, 673–681 (2010).
37. Huntenburg, J. M., Bazin, P.-L. & Margulies, D. S. Large-Scale Gradients in Human Cortical Organization. *Trends Cogn Sci* **22**, 21–31 (2018).
38. Goulas, A. *et al.* The natural axis of transmitter receptor distribution in the human cerebral cortex. *PNAS* **118**, (2021).
39. Rudolph, U. & Möhler, H. Analysis of GABAA Receptor Function and Dissection of the Pharmacology of Benzodiazepines and General Anesthetics Through Mouse Genetics. *Annual Review of Pharmacology and Toxicology* **44**, 475–498 (2004).
40. Ciric, R. *et al.* Mitigating head motion artifact in functional connectivity MRI. *Nat Protoc* **13**, 2801–2826 (2018).
41. Muschelli, J. *et al.* Reduction of motion-related artifacts in resting state fMRI using aCompCor. *Neuroimage* **96**, 22–35 (2014).
42. Margulies, D. S. *et al.* Situating the default-mode network along a principal gradient of macroscale cortical organization. *PNAS* **113**, 12574–12579 (2016).
43. Burt, J. B., Helmer, M., Shinn, M., Anticevic, A. & Murray, J. D. Generative modeling of brain

- maps with spatial autocorrelation. *NeuroImage* **220**, 117038 (2020).
44. Gryglewski, G. *et al.* Spatial analysis and high resolution mapping of the human whole-brain transcriptome for integrative analysis in neuroimaging. *NeuroImage* **176**, 259–267 (2018).
45. Masiulis, S. *et al.* GABA A receptor signalling mechanisms revealed by structural pharmacology. *Nature* **565**, 454–459 (2019).
46. Derry, J. M. C., Dunn, S. M. J. & Davies, M. Identification of a residue in the γ -aminobutyric acid type A receptor α subunit that differentially affects diazepam-sensitive and -insensitive benzodiazepine site binding. *Journal of Neurochemistry* **88**, 1431–1438 (2004).
47. Calkins, M. E. *et al.* The Philadelphia Neurodevelopmental Cohort: constructing a deep phenotyping collaborative. *J Child Psychol Psychiatry* **56**, 1356–1369 (2015).
48. Fogaça, M. V. & Duman, R. S. Cortical GABAergic Dysfunction in Stress and Depression: New Insights for Therapeutic Interventions. *Front. Cell. Neurosci.* **13**, (2019).
49. Yang, G. J. *et al.* Functional hierarchy underlies preferential connectivity disturbances in schizophrenia. *PNAS* **113**, E219–E228 (2016).
50. Sohal, V. S. & Rubenstein, J. L. R. Excitation-inhibition balance as a framework for investigating mechanisms in neuropsychiatric disorders. *Mol Psychiatry* **24**, 1248–1257 (2019).
51. Möhler, H. The GABA system in anxiety and depression and its therapeutic potential. *Neuropharmacology* **62**, 42–53 (2012).
52. Hubel, D. H. & Wiesel, T. N. Receptive fields of cells in striate cortex of very young, visually inexperienced kittens. *Journal of Neurophysiology* **26**, 994–1002 (1963).
53. Wiesel, T. N. & Hubel, D. H. SINGLE-CELL RESPONSES IN STRIATE CORTEX OF KITTENS DEPRIVED OF VISION IN ONE EYE. *J Neurophysiol* **26**, 1003–1017 (1963).
54. Wiesel, T. N. & Hubel, D. H. Extent of recovery from the effects of visual deprivation in kittens. *J Neurophysiol* **28**, 1060–1072 (1965).
55. Fagiolini, M. & Hensch, T. K. Inhibitory threshold for critical-period activation in primary

- visual cortex. *Nature* **404**, 183–186 (2000).
56. Caballero, A., Flores-Barrera, E., Thomases, D. R. & Tseng, K. Y. Downregulation of parvalbumin expression in the prefrontal cortex during adolescence causes enduring prefrontal disinhibition in adulthood. *Neuropsychopharmacology* **45**, 1527–1535 (2020).
57. Uhlhaas, P. J. *et al.* The development of neural synchrony reflects late maturation and restructuring of functional networks in humans. *Proc.Natl.Acad.Sci.U.S.A* **106**, 9866–9871 (2009).
58. Uhlhaas, P. J. & Singer, W. Abnormal neural oscillations and synchrony in schizophrenia. *Nat. Rev. Neurosci.* **11**, 100–113 (2010).
59. Ghisleni, C. *et al.* Subcortical Glutamate Mediates the Reduction of Short-Range Functional Connectivity with Age in a Developmental Cohort. *J. Neurosci.* **35**, 8433–8441 (2015).
60. Silveri, M. M. *et al.* Frontal Lobe γ -Aminobutyric Acid Levels During Adolescence: Associations with Impulsivity and Response Inhibition. *Biological Psychiatry* **74**, 296–304 (2013).
61. Balmer, T. S., Carels, V. M., Frisch, J. L. & Nick, T. A. Modulation of perineuronal nets and parvalbumin with developmental song learning. *J. Neurosci.* **29**, 12878–12885 (2009).
62. McRae, P. A., Rocco, M. M., Kelly, G., Brumberg, J. C. & Matthews, R. T. Sensory deprivation alters aggrecan and perineuronal net expression in the mouse barrel cortex. *J. Neurosci.* **27**, 5405–5413 (2007).
63. Bavelier, D., Levi, D. M., Li, R. W., Dan, Y. & Hensch, T. K. Removing brakes on adult brain plasticity: from molecular to behavioral interventions. *J. Neurosci.* **30**, 14964–14971 (2010).
64. Yakovlev, P. I., Lecours, A. R. & Minkowski, A. The myelogenetic cycles of regional maturation of the brain. in *Regional Development of the Brain in Early Life* 3–70 (Blackwell Scientific, 1967).
65. Grydeland, H., Walhovd, K. B., Tamnes, C. K., Westlye, L. T. & Fjell, A. M. Intracortical Myelin Links with Performance Variability across the Human Lifespan: Results from T1- and

- T2-Weighted MRI Myelin Mapping and Diffusion Tensor Imaging. *J. Neurosci.* **33**, 18618–18630 (2013).
66. Shafee, R., Buckner, R. L. & Fischl, B. Gray matter myelination of 1555 human brains using partial volume corrected MRI images. *Neuroimage* **105**, 473–485 (2015).
 67. Rowley, C. D. *et al.* Age-related mapping of intracortical myelin from late adolescence to middle adulthood using T1-weighted MRI. *Human Brain Mapping* **38**, 3691–3703 (2017).
 68. Corrigan, N. M. *et al.* Myelin development in cerebral gray and white matter during adolescence and late childhood. *NeuroImage* **227**, 117678 (2021).
 69. Vanes, L. D. *et al.* White matter tract myelin maturation and its association with general psychopathology in adolescence and early adulthood. *Human Brain Mapping* **41**, 827–839 (2020).
 70. Lebel, C. & Beaulieu, C. Longitudinal Development of Human Brain Wiring Continues from Childhood into Adulthood. *J. Neurosci.* **31**, 10937–10947 (2011).
 71. Simmonds, D. J., Hallquist, M. N., Asato, M. & Luna, B. Developmental stages and sex differences of white matter and behavioral development through adolescence: a longitudinal diffusion tensor imaging (DTI) study. *NeuroImage* **92**, 356–368 (2014).
 72. Pines, A. R. *et al.* Leveraging multi-shell diffusion for studies of brain development in youth and young adulthood. *Developmental Cognitive Neuroscience* **43**, 100788 (2020).
 73. Mauney, S. A. *et al.* Developmental pattern of perineuronal nets in the human prefrontal cortex and their deficit in schizophrenia. *Biol. Psychiatry* **74**, 427–435 (2013).
 74. Baker, K. D., Gray, A. R. & Richardson, R. The development of perineuronal nets around parvalbumin gabaergic neurons in the medial prefrontal cortex and basolateral amygdala of rats. *Behav. Neurosci.* **131**, 289–303 (2017).
 75. Paylor, J. W. *et al.* Developmental disruption of perineuronal nets in the medial prefrontal cortex after maternal immune activation. *Scientific Reports* **6**, srep37580 (2016).
 76. Drzewiecki, C. M., Willing, J. & Juraska, J. M. Influences of age and pubertal status on

- number and intensity of perineuronal nets in the rat medial prefrontal cortex. *Brain Struct Funct* (2020) doi:10.1007/s00429-020-02137-z.
77. Caspi, A. *et al.* Longitudinal Assessment of Mental Health Disorders and Comorbidities Across 4 Decades Among Participants in the Dunedin Birth Cohort Study. *JAMA Netw Open* **3**, e203221 (2020).
78. Paus, T., Keshavan, M. & Giedd, J. N. Why do many psychiatric disorders emerge during adolescence? *Nat Rev Neurosci* **9**, 947–957 (2008).
79. Sawada, T. *et al.* Developmental excitation-inhibition imbalance underlying psychoses revealed by single-cell analyses of discordant twins-derived cerebral organoids. *Molecular Psychiatry* **25**, 2695–2711 (2020).
80. Ghosal, S. *et al.* Ketamine rapidly reverses stress-induced impairments in GABAergic transmission in the prefrontal cortex in male rodents. *Neurobiology of Disease* **134**, 104669 (2020).
81. Fee, C. *et al.* Behavioral Deficits Induced by Somatostatin-Positive GABA Neuron Silencing Are Rescued by Alpha 5 GABA-A Receptor Potentiation. *International Journal of Neuropsychopharmacology* (2021) doi:10.1093/ijnp/pyab002.
82. Vollenweider, I., Smith, K. S., Keist, R. & Rudolph, U. Antidepressant-like properties of $\alpha 2$ -containing GABAA receptors. *Behavioural Brain Research* **217**, 77–80 (2011).
83. Ren, Z. *et al.* Bidirectional Homeostatic Regulation of a Depression-Related Brain State by Gamma-Aminobutyric Acidergic Deficits and Ketamine Treatment. *Biological Psychiatry* **80**, 457–468 (2016).
84. Luscher, B. & Fuchs, T. Chapter Five - GABAergic Control of Depression-Related Brain States. in *Advances in Pharmacology* (ed. Rudolph, U.) vol. 73 97–144 (Academic Press, 2015).
85. Sydnor, V. J. *et al.* Diminished reward responsiveness is associated with lower reward network GluCEST: an ultra-high field glutamate imaging study. *Molecular Psychiatry* 1–11

(2021) doi:10.1038/s41380-020-00986-y.

86. Fuchs, T. *et al.* Disinhibition of somatostatin-positive GABAergic interneurons results in an anxiolytic and antidepressant-like brain state. *Molecular Psychiatry* **22**, 920–930 (2017).
87. Insel, T. R. Mental disorders in childhood: shifting the focus from behavioral symptoms to neurodevelopmental trajectories. *JAMA* **311**, 1727–1728 (2014).
88. Wolf, D. H. *et al.* Amygdala abnormalities in first-degree relatives of individuals with schizophrenia unmasked by benzodiazepine challenge. *Psychopharmacology (Berl)* **218**, 503–512 (2011).
89. Satterthwaite, T. D. *et al.* Neuroimaging of the Philadelphia neurodevelopmental cohort. *Neuroimage* **86**, 544–553 (2014).
90. Satterthwaite, T. D. *et al.* The Philadelphia Neurodevelopmental Cohort: A Publicly Available Resource for the Study of Normal and Abnormal Brain Development in Youth. *Neuroimage* **124**, 1115–1119 (2016).
91. Esteban, O. *et al.* fMRIPrep: a robust preprocessing pipeline for functional MRI. *Nat Methods* **16**, 111–116 (2019).
92. Gorgolewski, K. *et al.* Nipype: A Flexible, Lightweight and Extensible Neuroimaging Data Processing Framework in Python. *Front. Neuroinform.* **5**, (2011).
93. Rastko Ćirić *et al.* *PennBBL/xcpEngine: atlas in MNI2009*. (Zenodo, 2020).
doi:10.5281/zenodo.4010846.
94. Tustison, N. J. *et al.* N4ITK: improved N3 bias correction. *IEEE Trans Med Imaging* **29**, 1310–1320 (2010).
95. Avants, B. B., Epstein, C. L., Grossman, M. & Gee, J. C. Symmetric diffeomorphic image registration with cross-correlation: evaluating automated labeling of elderly and neurodegenerative brain. *Med Image Anal* **12**, 26–41 (2008).
96. Jenkinson, M., Bannister, P., Brady, M. & Smith, S. Improved Optimization for the Robust and Accurate Linear Registration and Motion Correction of Brain Images. *NeuroImage* **17**,

- 825–841 (2002).
97. Cox, R. W. AFNI: software for analysis and visualization of functional magnetic resonance neuroimages. *Comput. Biomed. Res.* **29**, 162–173 (1996).
98. Glasser, M. F. *et al.* The minimal preprocessing pipelines for the Human Connectome Project. *Neuroimage* **80**, 105–124 (2013).
99. Greve, D. N. & Fischl, B. Accurate and robust brain image alignment using boundary-based registration. *Neuroimage* **48**, 63–72 (2009).
100. Satterthwaite, T. D. *et al.* An improved framework for confound regression and filtering for control of motion artifact in the preprocessing of resting-state functional connectivity data. *NeuroImage* **64**, 240–256 (2013).
101. Woolrich, M. W., Ripley, B. D., Brady, M. & Smith, S. M. Temporal autocorrelation in univariate linear modeling of fMRI data. *Neuroimage* **14**, 1370–1386 (2001).
102. Fair, D. A. *et al.* A method for using blocked and event-related fMRI data to study “resting state” functional connectivity. *NeuroImage* **35**, 396–405 (2007).
103. Schaefer, A. *et al.* Local-Global Parcellation of the Human Cerebral Cortex from Intrinsic Functional Connectivity MRI. *Cereb Cortex* **28**, 3095–3114 (2018).
104. Tzourio-Mazoyer, N. *et al.* Automated Anatomical Labeling of Activations in SPM Using a Macroscopic Anatomical Parcellation of the MNI MRI Single-Subject Brain. *NeuroImage* **15**, 273–289 (2002).
105. Glasser, M. F. *et al.* A multi-modal parcellation of human cerebral cortex. *Nature* **536**, 171–178 (2016).
106. Gordon, E. M. *et al.* Generation and Evaluation of a Cortical Area Parcellation from Resting-State Correlations. *Cereb. Cortex* (2014) doi:10.1093/cercor/bhu239.
107. Cortes, C. & Vapnik, V. Support-vector networks. *Mach Learn* **20**, 273–297 (1995).
109. Meyer, D. *et al.* e1071: Misc Functions of the Department of Statistics, Probability Theory Group (Formerly: E1071), TU Wien. (2020).

110. Mourão-Miranda, J., Bokde, A. L. W., Born, C., Hampel, H. & Stetter, M. Classifying brain states and determining the discriminating activation patterns: Support Vector Machine on functional MRI data. *NeuroImage* **28**, 980–995 (2005).
111. Rudolph, U. & Knoflach, F. Beyond classical benzodiazepines: novel therapeutic potential of GABA A receptor subtypes. *Nature Reviews Drug Discovery* **10**, 685–697 (2011).
112. Hawrylycz, M. J. *et al.* An anatomically comprehensive atlas of the adult human brain transcriptome. *Nature* **489**, 391–399 (2012).
113. Simpson, G. L. Modelling Palaeoecological Time Series Using Generalised Additive Models. *Front. Ecol. Evol.* **6**, (2018).
114. Simpson, G. L. & Singmann, H. *gratia: Graceful 'ggplot'-Based Graphics and Other Functions for GAMs Fitted Using 'mgcv'*. (2021).
115. Castro-Schilo, L. & Grimm, K. J. Using residualized change versus difference scores for longitudinal research. *Journal of Social and Personal Relationships* **35**, 32–58 (2018).
116. Wood, S. N. *Generalized Additive Models: An Introduction with R, Second Edition*. (Chapman and Hall/CRC, 2017). doi:10.1201/9781315370279.
117. Shanmugan, S. *et al.* Common and Dissociable Mechanisms of Executive System Dysfunction Across Psychiatric Disorders in Youth. *Am J Psychiatry* **173**, 517–526 (2016).
118. Kaczkurkin, A. N. *et al.* Evidence for Dissociable Linkage of Dimensions of Psychopathology to Brain Structure in Youths. *AJP* **176**, 1000–1009 (2019).